Broadband Characterization of Coplanar Waveguide Interconnects With Rough Conductor Surfaces

Arghya Sain, *Member, IEEE*, and Kathleen L. Melde, *Fellow, IEEE*

***Abstract*— This paper presents a method to simulate the effects of conductor surface roughness on conductor-backed coplanar waveguide (CB-CPW) interconnects using 3-D full wave simulation tools. In this paper, a high-frequency structure simulator (HFSS) from ANSYS has been implemented for rough surfaces with Gaussian correlation functions. The rough surfaces that exist between the dielectric and copper foils are modeled using a statistical random process approach. The varying heights for the random rough surface with specified autocorrelation function (ACF), root mean square height ($H_{\rm rms}$), and correlation length (λ) are generated using MATLAB, and these data are used in HFSS to model and simulate the performance of the CB-CPW interconnect with rough conductor surfaces. The results show that both $H_{\rm rms}$ and λ influence the overall attenuation coefficient, and the trends are consistent with the other studies in this area. The method presented in this paper provides designers with a technique to characterize the effect of conductor surface roughness for different types of transmission lines with varying substrates and extent of conductor roughness.**

***Index Terms*— Autocorrelation function (ACF), conductor-backed coplanar waveguide (CB-CPW), conductor loss, interconnect, power spectral density (PSD), root mean square height (H_{rms}), surface roughness, transmission lines.**

I. Introduction

THE geometric dimensions of transmission line interconnects are shrinking as engineers design smaller and faster systems by moving into the high-frequency regime. Transmission lines operating at high frequencies see an increase in resistive losses that can adversely affect the performance of the electrical system. For smooth conductors, the series resistance increase with frequency is attributed to the skin depth, which is inversely proportional to the square root of frequency. In practice, the conductor surfaces are roughened by the manufacturers to promote adhesion between the dielectric and conductors in printed circuit boards. The 90° peel strength is a measure of how well a conductor adheres to the dielectric material and is directly proportional to the fourth root of the thickness of deformed resin (y_o) and other parameters like foil thickness, etc. [1]. Intentional roughening of the surface between the copper foil and dielectric improves peel strength and adhesion between the metal and dielectric. Conductor surface roughness increases resistive losses at higher frequencies, affecting signal integrity. The skin depth decreases with increasing signal frequency and becomes comparable to the localized peaks of the roughened conductor surface. The current follows the surface undulations of the rough conductor, which increases the effective path length and reduces the cross-sectional area of current flow, resulting in increased resistance. Experimental results show that rough conductors exhibit 10%–50% higher losses compared to that of smooth conductors [2]. High conductor surface roughness also increases dispersion and effective dielectric constant by up to 15% [3].

This paper presents a way for designers to create frequency-domain models and to quantify these effects in their designs. A traditional way to account for the rough conductor losses in transmission lines is through the use of the Hammerstad equation

$$R = K_H R_s \sqrt{f} \tag{1}$$

where $R_s\sqrt{f}$ is the skin depth resistance for a smooth conductor, and K_H is called the Hammerstad coefficient given by

$$K_H = 1 + \frac{2}{\pi}\arctan\left[1.4\left(\frac{H_{\rm rms}}{\delta}\right)^2\right] \tag{2}$$

where δ is the skin depth and $H_{\rm rms}$ is the root mean square value of the surface roughness height [4], [5]. The Hammerstad model is not applicable when operating frequencies are greater than 5 GHz because it is based on a 2-D corrugated surface for the copper foil and should be used for conductor foils with $H_{\rm rms} \leq 2\ \mu$m [5]. To fill this void, a hemispherical model was introduced with a new correction factor $K_{\rm Hemi}$ that replaces K_H in (1). The hemispherical model levels off at a much higher value compared to the Hammerstad model, which always levels off at a value of two. The hemispherical model is an improvement over the Hammerstad model, but it still over and under predicts loss at middle and high frequencies, respectively, and it is valid for very specific conductor profiles [5], [6]. Scanning electron microscope (SEM) images show pyramid-like structures formed by electrodeposited (ED) copper spheres (snowballs) [4]–[6].

The Huray model was introduced after the hemispherical model. This model includes the Huray surface roughness correction factor ($K_{\rm Huray}$), which replaces K_H in (1). Such a structure is extremely difficult to model for simulation in 3-D electromagnetic full wave solvers because the SEM images need to be analyzed very closely to determine

Manuscript received June 27, 2012; revised November 7, 2012; accepted January 12, 2013. Date of publication April 25, 2013; date of current version May 29, 2013. This work was supported in part by the National Science Foundation under Grant ECCS-1231368, the Semiconductor Research Corporation Task 1292.063, and the Army Research Office under Contract WN911NF-12-1-0155. Recommended for publication by Associate Editor R.-B. Wu upon evaluation of reviewers' comments.

The authors are with the Department of Electrical and Computer Engineering, University of Arizona, Tucson, AZ 85721 USA (e-mail: asain@email.arizona.edu; melde@email.arizona.edu).

Color versions of one or more of the figures in this paper are available online at http://ieeexplore.ieee.org.

Digital Object Identifier 10.1109/TCPMT.2013.2243803

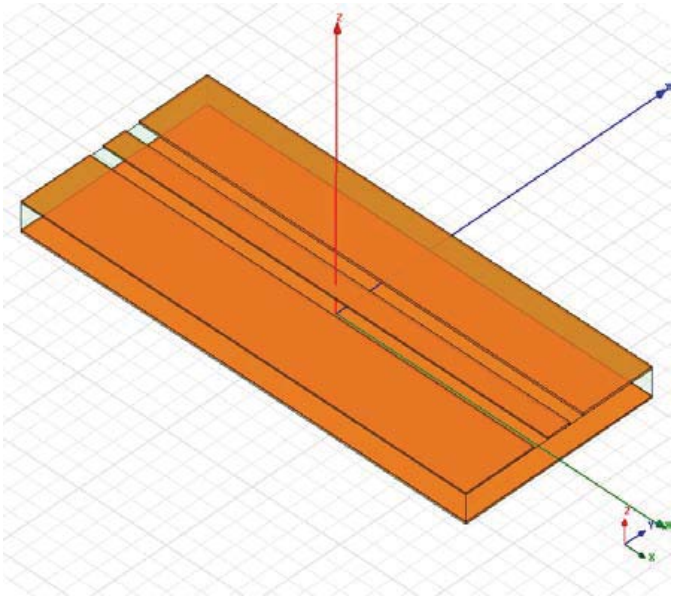

Fig. 1. Conductor-backed coplanar waveguide. The direction of signal propagation is along the x-axis.

snowball dimensions and the number of spheres in each protrusion. Such data are not readily available from the manufacturers. The effects of conductor random rough surface on attenuation have been studied for 2-D and 3-D cases using the small perturbation method second order (SPM2) and the method of moments (MoM) [7], [8]. These methods rely on a 2-D surface model that has limited accuracy since the power absorption ratio increases significantly with 3-D configurations. The SPM2 applies to surfaces with small levels of roughness [9]. The authors in [9] have developed a scalar-wave model (SWM) to simulate the effect of 3-D surface roughness over diverse roughness profiles over a wide frequency band. Much of the prior work is focused on microstrip lines with specific rough surface conductor profiles and relies on simulation software that is not broadly available in the industry. There is no published technique that discusses simulating the effect of conductor surface roughness on different types of transmission lines using 3-D full wave electromagnetic field solvers.

This paper presents a general way of simulating the effects of conductor surface roughness for CB-CPW using ANSYS high-frequency structure simulator (HFSS) [10]. A CPW on a dielectric substrate consists of a central conductor (signal) with finite width ground planes on either side. CB-CPW has an additional ground plane at the bottom surface of the substrate as shown in Fig. 1. The CB-CPW supports a low-dispersion quasi-TEM mode of propagation [11]. The conductor backing below the CPW adds additional shielding for interconnects that may be routed below the CB-CPW in the case of multilayer modules. CB-CPWs simplify fabrication by facilitating easy surface mounting or flip-chip attachment of active and passive devices. CB-CPW allows the use of automatic on-wafer measurements for interconnection of components and characterization. CB-CPW circuits have a ground plane between two adjacent lines reducing cross talk. This paper presents a way to analyze the effects of conductor roughness on CB-CPWs for different roughness parameters and validates the simulation results with published results in the literature. This methodology is applicable to other rough surface profiles and different types of transmission lines. The advantage of this approach is that designers are often familiar with interconnect modeling of smooth lines in HFSS, and thus existing design cases may be utilized to include the effects of surface roughness.

The results presented here are based on CB-CPW on copper clad Megtron6. The dielectric thickness is 254 μm, the width of the signal trace is 254 μm, and the width of the gap between signal line and the coplanar ground traces is 58.42 μm. The thickness and conductivity of the conductor is 17.78 μm and 5.8×10^7 S/m, respectively. The relative permittivity of the substrate is 3.5. In this paper, no vias between the top ground and lower ground conductors were used. An absorbing boundary condition was placed up against the edges of the top layer ground planes in order to create an ideal CB-CPW. Simulations were run to verify that only the CB-CPW mode propagates all the way up to 40 GHz. No unusual mode behavior, such as even or odd propagating modes or signal loss, was observed.

The surface roughness modeling approach is based upon implementing the characteristics of the rough surface model directly into full wave electromagnetic simulators, such as HFSS. HFSS solves Maxwell's equations directly using the finite element method (FEM). HFSS has been used to compute the electric field scattering off rough dielectric surfaces for calculating the scattering coefficients and emissivity of such dielectric mediums [12]. The HFSS results are in close agreement with the MoM, predicted and published measured results to 40 GHz.

A method of generating rough conductor surfaces with the desired root mean square height, correlation length, and surface correlation function is discussed and implemented. This technique allows one to simulate the effects of surface roughness on different types of transmission lines. Previous studies provide insight into the variation of either insertion loss or attenuation coefficient (or enhancement factor) with frequency. This new method provides access to both parameters simultaneously for up to 40 GHz. Interconnect performance can be better understood via the field plots in the interconnects. Section II deals with the different properties of the random rough surfaces.

II. Random Rough Surfaces

A random rough surface is modeled as a stationary random process with zero mean and is characterized by the root mean square height (H_{rms}), correlation length (λ), and autocorrelation function (ACF) [8], [13]. While two rough surfaces can have the same statistical parameters, the physical profiles are not necessarily the same. The height probability distribution function of a rough surface is assumed to be a Gaussian distribution with zero mean and H_{rms} as the standard deviation. Additional details are described in [13] and [14].

Copper foils used as conductors in transmission lines can be broadly classified into three types: rolled annealed (RA),

reverse treated (RT), and ED. $H_{\rm rms}$ ranges from 0.4 to 0.5 μm, 0.5 to 0.7 μm, and 1 to 4 μm for RA, RT, and ED foils respectively. The ED foils can be hyper very low profile (1.5 μm $\leq$ $H_{\rm rms}$ $\leq$ 2 μm) and very low profile (3 μm $\leq H_{\rm rms} \leq$ 4 μm) [3], [15]. This is consistent with the finding in [4], which says, $H_{\rm rms}$ varies from 0.3 to 5.8 μm. The correlation length is defined as the distance over which the ACF falls by $1/e$. λ varies between 0.3 and 3.5 μm [7], [9].

Different random surfaces are distinguished by their ACFs, which determine the extent of roughness of the surface. For conductor surfaces, the ACFs are either Gaussian or exponential in nature. The exponential surface correlation function is rougher than the Gaussian ACF for a given $H_{\rm rms}$ and λ [7]. The random rough surfaces are assumed to be isotropic, stationary (translational invariance), and ergodic. A rough surface is defined as isotropic if the statistical nature of the surface is independent of the direction along the surface [13]. The isotropic nature of the rough surfaces results in λ being equal in two perpendicular directions. Theoretically, given $H_{\rm rms}$, λ, and ACF, a large number of unique rough surfaces can be created. Consider that the direction of propagation of signal in a CB-CPW is along the x-axis. A normalized Gaussian correlation function is represented as in [7]

$$C\left(x, y\right) = \exp\left(-\frac{x^2 + y^2}{\lambda^2}\right). \tag{3}$$

The Fourier transform of an ACF results in the power spectral density (PSD) function, which is another way of describing the rough surface in the spatial domain. In the case of the Gaussian ACF, the PSD is also Gaussian, given by

$$P\left(k_x, k_y\right) = \frac{H_{\rm rms}^2 \lambda^2}{4\pi} \exp\left(-\frac{\left(k_x^2 + k_y^2\right)\lambda^2}{4}\right). \tag{4}$$

The exponential ACF and PSD are represented as follows:

$$C\left(x, y\right) = \exp\left(-\frac{\sqrt{x^2 + y^2}}{\lambda}\right) \tag{5}$$

$$P\left(k_x, k_y\right) = \frac{H_{\rm rms}^2 \lambda^2}{2\pi} \frac{1}{\left\{1 + \left(k_x^2 + k_y^2\right)\lambda^2\right\}^{3/2}}. \tag{6}$$

This paper considers the Gaussian surface correlation function. To capture the behavior of the exponentially correlated rough surface, the sampling interval should be at least one-tenth of λ, which is too intensive a simulation to handle for the time being [13].

III. Generating a Random Rough Surface

A randomly roughened 3-D surface with Gaussian height distribution and any given surface correlation function can be generated via the linear transformation of matrices, whose components are Gaussian random numbers with zero mean and a standard deviation of one [16]. To use this, one needs to numerically solve a set of simultaneous nonlinear equations for determining the transform coefficients. A much more efficient method of generating 3-D rough surfaces with various

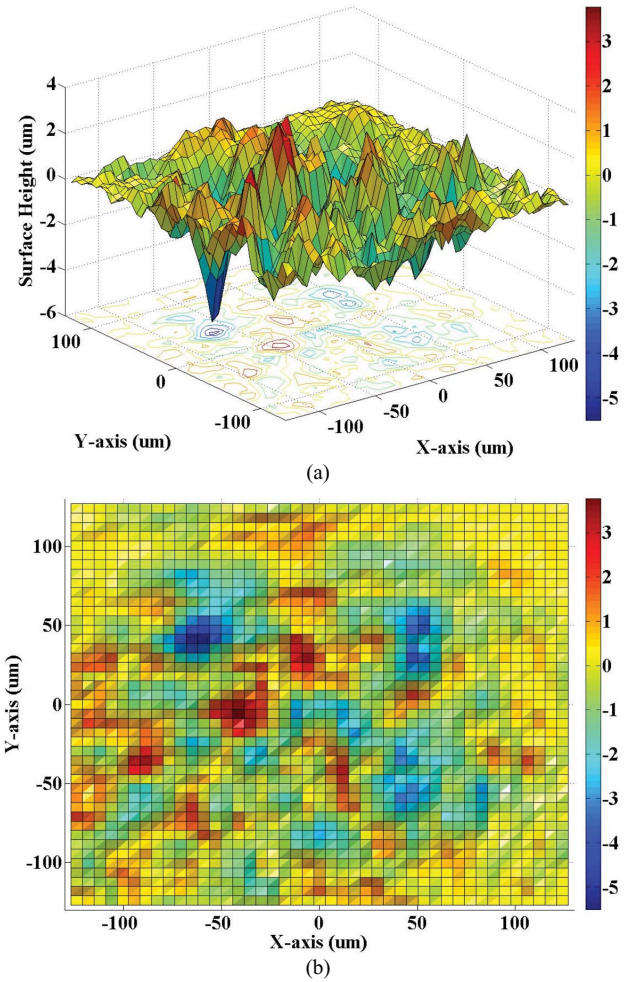

Fig. 2. (a) Random rough surface with $H_{\rm rms}$ = 5.5 and λ = 3 μm. (b) Contour plot of the same surface.

ACFs is using the techniques of digital filter design [17]. This method uses an independent Gaussian distribution of random numbers of zero mean and unity standard deviation, that is generated using the random number generator functions built in MATLAB [18], for a mesh of points on the X–Y surfaces. This vector is convolved with the Gaussian ACF and then normalized and multiplied with $H_{\rm rms}$ to obtain the random surface heights with the desired surface characteristics [17], [19]. This process is given by

$$z\left(r\right) = H_{\rm rms}\left[\text{normalized}\left\{\iint_{-\infty}^{\infty} C\left(r - r'\right) \times Z\left(r'\right) dr'\right\}\right] \tag{7}$$

where $z(r)$ represents the random surface heights, $r = (x, y)$ and $Z(r)$ is the set of random numbers. Equation (7) can also be solved using fast Fourier transform and the Gaussian PSD is used instead of the Gaussian ACF. The random rough surface is shown in Fig. 2.

The shapes of the rough surface on the copper foil obtained from surface profile measurements and SEM (from [4] and [6]) have a conical shape. Thus, the model in this paper uses varying heights of the rough surfaces as cones of randomly

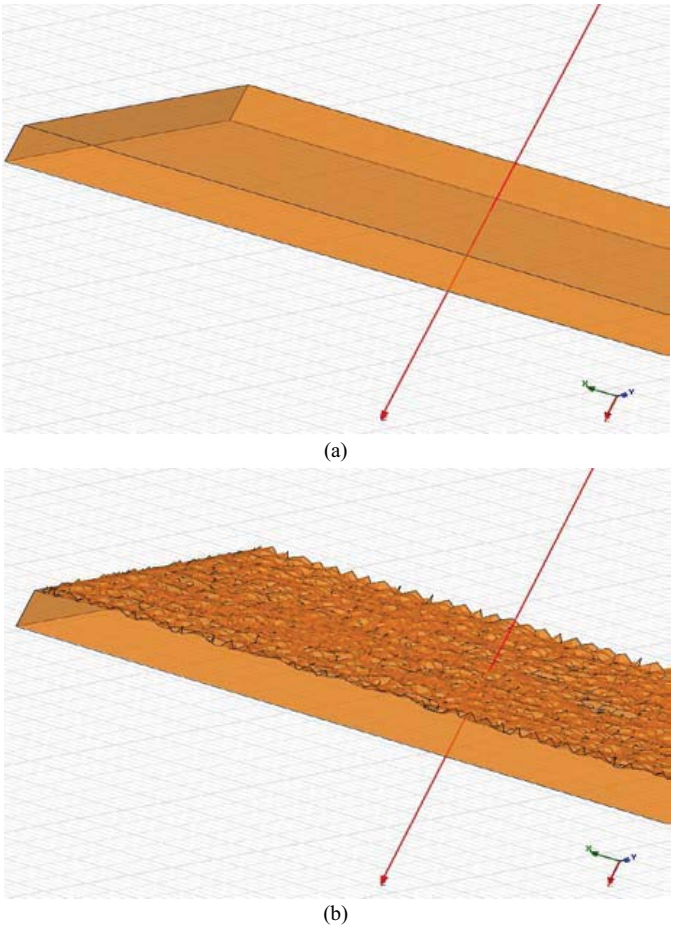

Fig. 3. Signal conductor with (a) smooth surface and (b) randomly roughened surface. Only the surface of the conductor making contact with the substrate is roughened.

varying heights and diameters. $z(r)$ obtained from (7) sets the cone heights, while the radii are set using another set of random numbers generated in MATLAB. The random number data are stored in an Excel sheet along with the coordinates for the cones. A visual basic (VB) script is used to create a 50-Ω CB-CPW geometry with smooth conductor surfaces that can be imported into HFSS. The VB script reads the Excel file to modify the geometry to include surface roughness. The file includes the data of the randomly generated cones for the conductors on the signal and grounds. The script unites the cones to the smooth conductor surfaces. The script also ensures that in the overall geometry file a portion of dielectric material is subtracted (or added) to create a continuous interface that mimics the roughness profile between the substrate and the conductor. Special care was taken to appropriately set the zero mean to the mountains and valleys in the roughened profile. The interface between the conductor and substrate is roughened, while the interface between conductor and air is kept smooth. A small segment of CB-CPW with smooth conductors is added to each end in order to prevent nonuniform, nonplanar surfaces from touching the waveports, which is necessary for a waveport excitation in HFSS.

Since the roughened conductor geometry presents a complex tetrahedral meshing challenge, a study was conducted to investigate the impact of how limiting the area of roughened conductors in the model affects accuracy and computational load. Roughening all conductor surfaces results in long simulation times. The study showed that the conductor surfaces that experience the highest current density and greatest E-field should be roughened. Specifically, the finite width side ground conductors on the signal layer, the signal conductor, and the area of the bottom ground plane that is directly under the signal conductor should be rough. The structure is simulated over a frequency range of 1–40 GHz in discrete frequency steps of 1 GHz with 40 GHz as the solution (or meshing) frequency. A comparison of the smooth to rough conductor surface generated by the above process is shown in Fig. 3.

IV. Results and Comparison

In this section, we will see how H_{rms} and λ influence the losses in CB-CPWs. The enhancement factor (k) is defined as the ratio of the attenuation coefficient of a rough surface to that of a smooth surface. The trends observed in the variation of enhancement factor and insertion loss match the results presented in [3], [4], and [7]. We see that the enhancement factor neither saturates nor shows any trend of saturation at higher frequencies. The attenuation and insertion loss increases with increased conductor roughness.

In the first case, we simulated two interconnects with constant H_{rms} (1 μm) with $\lambda = 1$ and 4 μm, respectively. The results are shown in Fig. 4. The results show that the attenuation coefficient falls with increasing correlation length. Note that increasing the correlation length results in a smoother conductor surface profile. The enhancement factor for $\lambda = 1$ μm is higher than $\lambda = 4$ μm, indicating higher attenuation. This suggests an increase in the roughness of the surface with decreasing λ. The insertion loss for both cases is essentially the same, and suggests that λ alone may not be a dominating factor in determining the extent of attenuation.

Fig. 5 shows the results when H_{rms} is varied from 1 to 5.5 μm with λ being held constant at 3 μm. The results show that for this case, the attenuation coefficient increases with increasing root mean square height. Increasing root mean square height results in a rougher conductor surface profile. These figures show that increasing H_{rms} creates a rougher surface and thus, increases resistive losses. While there does not seem to be a huge difference in the insertion loss, the proliferation of low-power electrical circuits is increasing, and this means even a slight variation in power can cause a shift in the logic state of the devices, resulting in unpredictable errors.

Fig. 6 shows the simulated results for the case where both H_{rms} and λ are varied. The results suggest that H_{rms} affects the results more than λ, thus deciding the extent of the resistive losses suffered by a transmission line. Increasing H_{rms} and decreasing λ indicate an increase in the roughness profile of a surface. In this case, both the root mean square height and correlation length are varied at the same time by the same amount ($H_{\text{rms}} = \lambda$). We see that the attenuation coefficient and enhancement factor both increased with increasing H_{rms} and λ as in Fig. 6(a) and (b).

A review of these results in the context of the law of conservation of energy provides some additional insight.

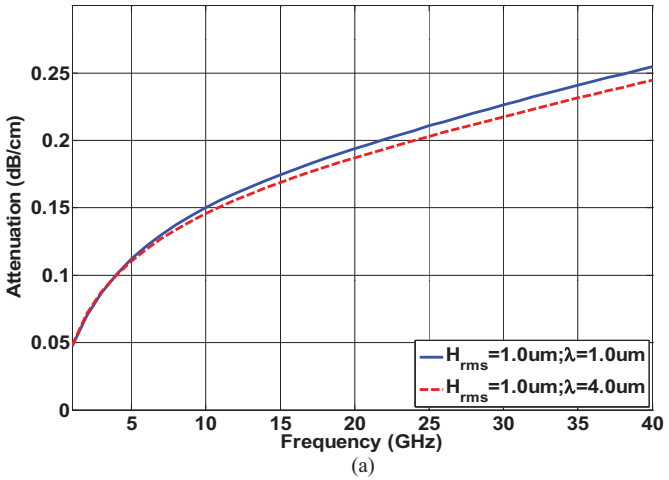

(a)

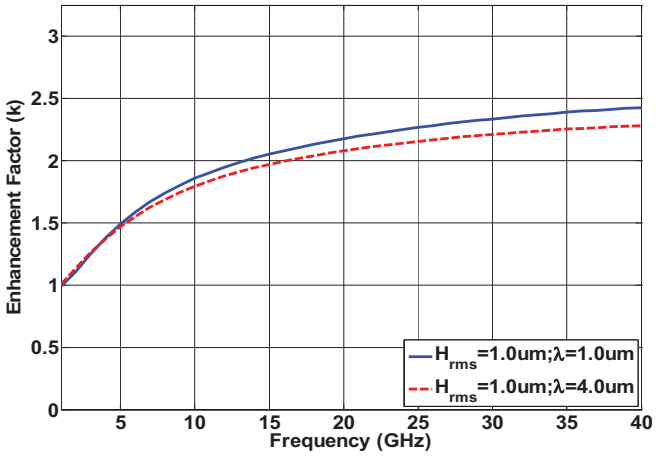

(b)

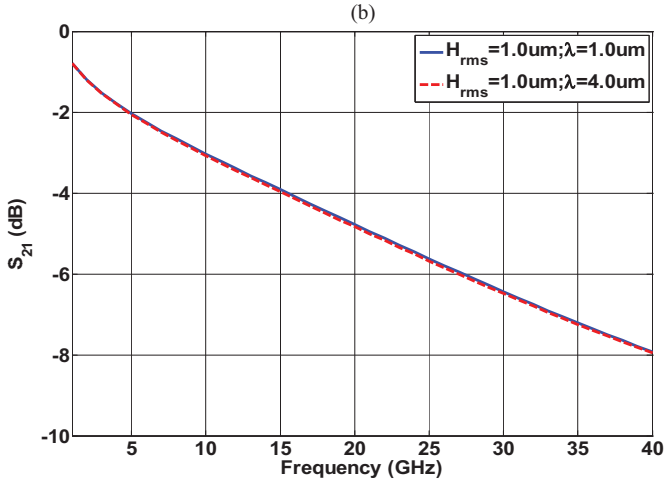

(c)

Fig. 4. (a) Attenuation coefficient per unit length, (b) enhancement factor, and (c) insertion loss as a function of frequency for varying λ (1.0 and 4.0 μm) and constant $H_{\rm rms}$ (1.0 μm) for a 7-in-long CB-CPW.

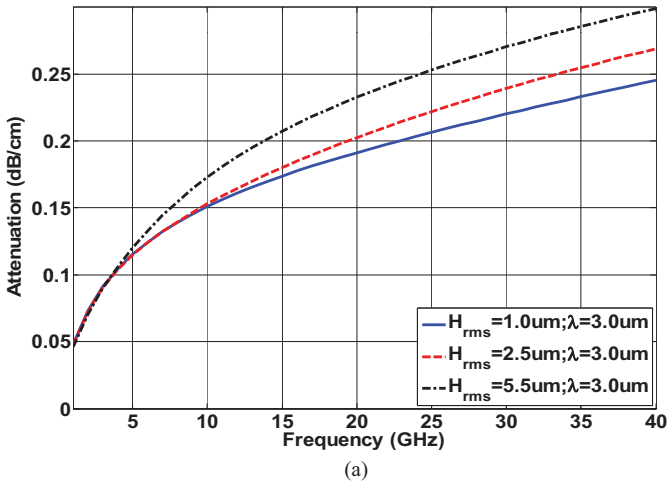

(a)

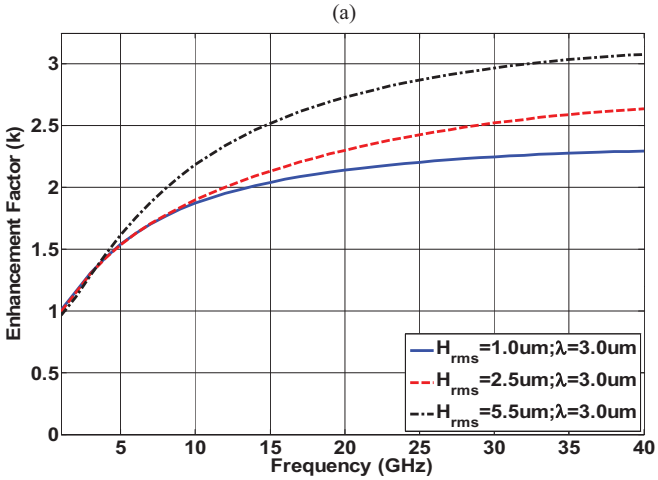

(b)

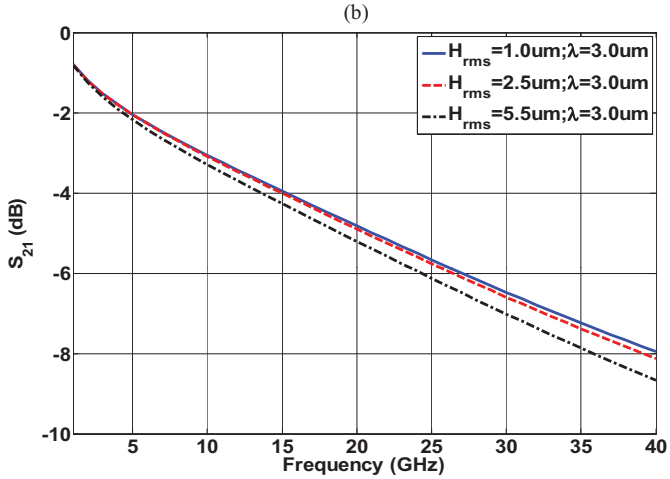

(c)

Fig. 5. (a) Attenuation coefficient per unit length, (b) enhancement factor, and (c) insertion loss as a function of frequency for constant λ (3.0 μm) and varying $H_{\rm rms}$ (1.0, 2.5, and 5.5 μm) for a 7-in-long CB-CPW.

A current passing through a conductor results in a magnetic field (creating inductance) that surrounds the conductor, according to the right-hand rule. According to [4], the total inductance in a current-carrying conductor is the sum of external and internal inductances, denoted by $L_{\rm ext}$ and $L_{\rm int}$, respectively. $L_{\rm int}$ and $L_{\rm ext}$ are caused by current flowing inside and on the surface of the conductor, respectively. Total inductance is reduced by $L_{\rm int}$ at high frequencies as current in the conductor is confined to the surface. Consequently, the associated magnetic field has reduced energy-storage capacity. Therefore, the excess energy that can no longer be stored in the magnetic field must be dissipated by resistive losses (skin effect), thus increasing attenuation at high frequencies.

In order to validate the simulated results, a comparison with published and measured results was conducted. No studies that provided sufficient details on the material samples

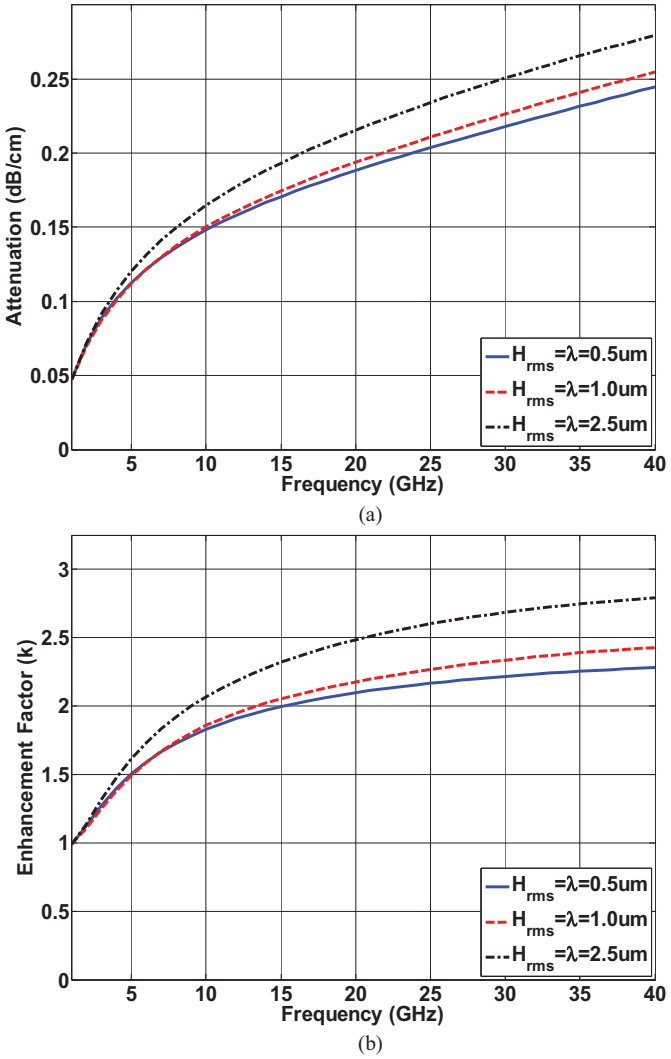

Fig. 6. (a) Attenuation coefficient per unit length and (b) enhancement factor loss as a function of frequency for varying λ and $H_{\rm rms}$($H_{\rm rms} = \lambda$; 0.5, 1.0, and 2.5 μm) for a 7-in-long CB-CPW.

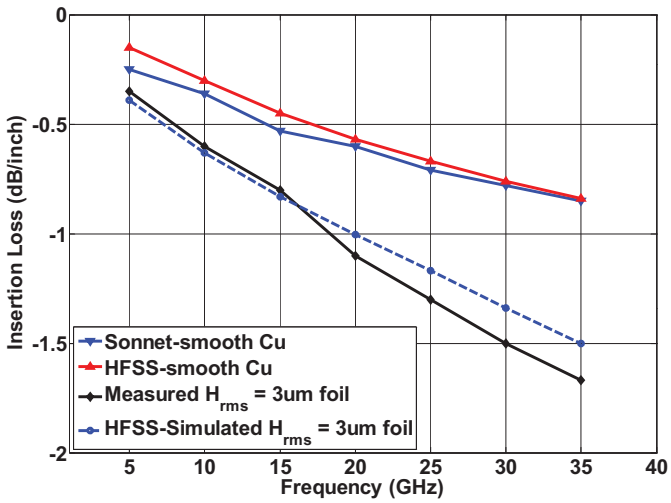

Fig. 7. Comparison of measured results from [3] with simulated results from HFSS.

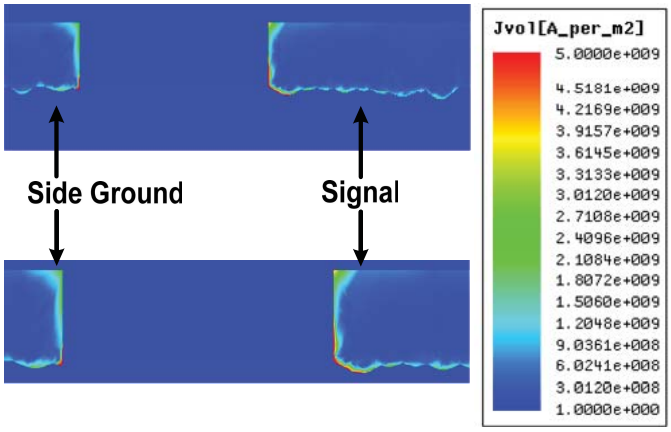

Fig. 8. Cross-sectional view of current distribution in (a) portions of roughened signal and side ground and (b) zoomed in image of a portion of the roughened conductors in (a) at 40 GHz. The plots are in linear scale. The smooth signal is 17.78-μm thick. The current is flowing into the plane of this paper.

were found for CB-CPW. A detailed study that includes both measured and simulated insertion loss with and without surface roughness for microstrip transmission lines was used [3]. HFSS simulation models for 50-Ω microstrip lines on 100-μm-thick Rogers ULTRALAM 3850 LCP substrate using 18-μm-thick copper lines with and without surface roughness were created. The models with rough conductor surfaces use the same methodology discussed in Section III. The substrate has a loss tangent and dielectric constant of 0.0025 and 2.9, respectively, at 10 GHz. Two cases were simulated in HFSS. The first one is a microstrip line without any conductor roughness, and the second one is with conductor surface roughness with $H_{\rm rms} = 3$ and $\lambda = 1$ μm. The simulated and measured results are shown in Fig. 7. The plots with name "HFSS-smooth Cu" and "HFSS-Simulated $H_{\rm rms}$ = 3-μm foil" are the two test cases we simulated, while the plots "Sonnet-smooth Cu" and "Measured $H_{\rm rms}$ = 3-μm foil" are from [3]. We see a good correlation between the measured and simulated data within the limits of experimental errors. There is an average difference of 0.6% and 1.2% between the results computed by our method and the comparison data, for the smooth and rough copper foils, respectively. Note, measured data on smooth foils are not available.

The next step is to look at the current distribution on the conductor surfaces. Fig. 8 shows how the current on the conductors follows the surface contours of the rough surfaces. Fig. 8(a) shows the current distribution in the cross-sectional slice of a portion of the signal conductor and one-side ground for the roughened conductor surfaces. Fig. 8(b) shows the same view, but zoomed in. The current is flowing into the plane of the page (i.e., along the length of the transmission line). The figures clearly show that the interface between the conductor and the substrate is roughened. Both plots use the same linear scale. The figures even show the appropriate current density behavior consistent with the edge effect [20]. In practice, the lines are trapezoidal in cross section with the line width at top less than that at the bottom (metal substrate interface), since in wet etching the etchant has more time to interact with metal at

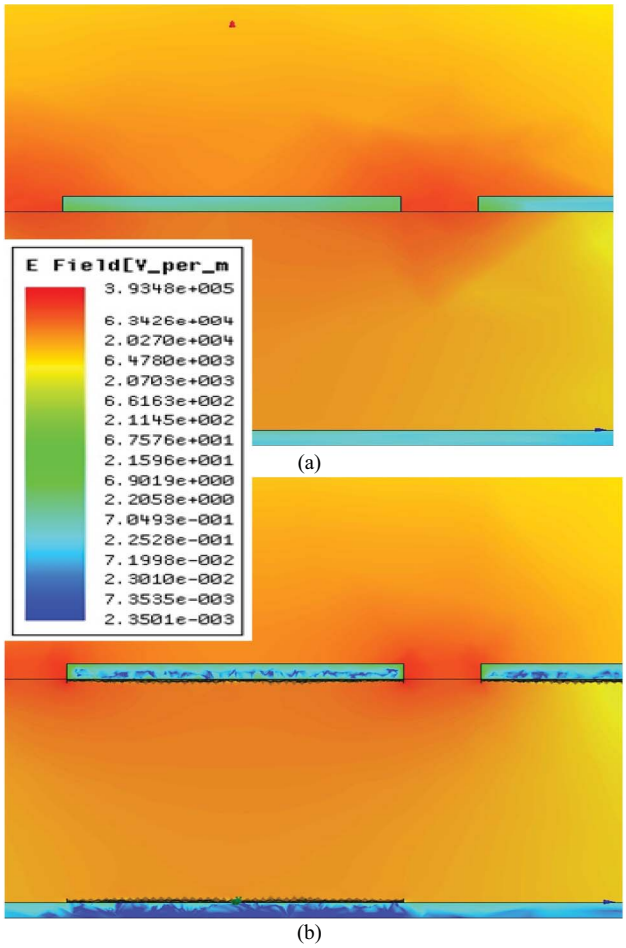

Fig. 9. Cross-sectional view of the electric field distribution in CB-CPW with (a) smooth and (b) rough conductor surfaces at 40 GHz, in log scale.

top. The edges of transmission lines also exhibit roughness that is dependent upon the circuit fabrication process. These factors will also create higher insertion loss, which could account for some measurement and simulation differences in Fig. 7. The impact of these factors is beyond the scope of this paper.

Fig. 9 shows how the electric field inside the conductor falls off due to the presence of the rough structure when compared to the conductor with a smooth surface. The variation in the depth of penetration of the electric field can be attributed to the randomness of the thickness of the conductors. Fig. 9 shows the electric field distribution in the cross section of the CB-CPW with smooth and rough conductor surfaces at 40 GHz. The electric field is plotted in log scale. The electric field pattern in the dielectric and the air; however, remains unperturbed even in the presence of the rough conductor surface.

V. Computational Requirements and Model Generation

This section discusses some of the factors involved in creating the HFSS models and a comparison of approaches used to reduce the computational complexity of the rather detailed rough surface geometries. First, a study of the FEM mesh created by HFSS was conducted. Fig. 10 shows the FEM

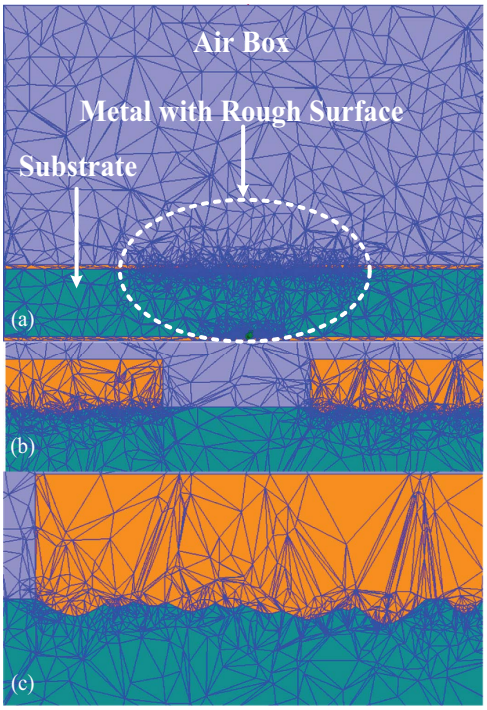

Fig. 10. Cross-sectional view of the mesh generated in HFSS. (a) Meshing in the entire cross section of the device. (b) Meshing in the metal (signal and side ground) with a roughened surface. (c) Zoomed in image of the meshing at the signal conductor with the roughened surface clearly visible.

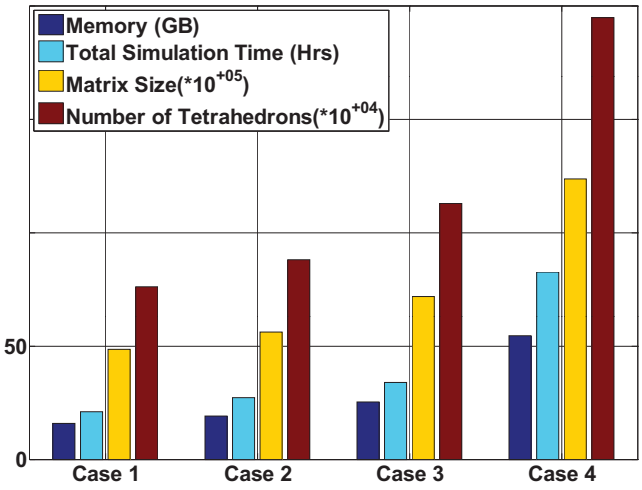

Fig. 11. Bar plot for memory, simulation time, matrix size and number of tetrahedrons for CB-CPWs with varying extents of conductor surface roughness.

mesh at the cross section of the line. Fig. 10(a) shows the airbox region surrounding the line, and the lower region is the Megtron6 substrate sandwiched between the copper surfaces. Fig. 10(a) shows the mesh generated at one cross section of the entire structure. The mesh is very dense in the areas where the conductors have been roughened. This region is shown with a white dotted circle in Fig. 10(a). Fig. 10(b) shows a zoomed in image of the mesh in the region around one of the side grounds and the signal, and Fig. 10(c) shows a further zoomed in image of the meshing in the region underneath the roughened signal.

Another interesting aspect of this paper involves the computational power required to perform such simulations. All these simulations were performed on an Intel Xeon system with 12 cores distributed across two physical processors and 256 GB of random access memory (RAM). The operating system installed is Windows Server 2008 R2 enterprise. Four cases were considered: Case 1 ($H_{\text{rms}} = \lambda = 0.5\ \mu$m), Case 2 ($H_{\text{rms}} = \lambda = 1.0\ \mu$m), Case 3 ($H_{\text{rms}} = \lambda = 2.5\ \mu$m), and Case 4 ($H_{\text{rms}} = 5.5\ \mu$m; $\lambda = 3.0\ \mu$m). Each case is further subdivided into four categories, namely memory [peak amount of physical memory (RAM) used], total simulation time, matrix size (number of unknowns), and number of tetrahedrons. RAM usage, matrix size, and number of tetrahedrons increase with each adaptive pass until convergence. Once the adaptive pass has converged, the RAM usage, matrix size, and the number of tetrahedrons become constant over the entire frequency range. It becomes clear from Fig. 11 that computational complexity and time increase with the increase in roughness of the surface.

VI. Conclusion

In this paper, a technique to design conductor surface roughness for CB-CPWs using 3-D full-wave electromagnetic field solvers like HFSS was presented. The simulation results suggest an increase in attenuation and thus enhancement factor and insertion loss as the roughness of the conductors increased with increasing frequency. Unlike the Hammerstad model, the enhancement factor did not saturate at two; instead, the enhancement factor continued to increase with increasing frequency for any given rough surface. H_{rms} played a dominant role when compared to λ. The roughness of a surface increases as H_{rms} increases and λ decreases. The trends seen in the enhancement factor and the insertion loss for the different cases followed the trends presented in the references. Some differences were expected, given that the materials and transmission lines used in the references are different. The simulations also helped provide a clear picture of the current distribution in the signal conductor. The increase in computational complexity with the increase in surface roughness of the conductors in the CB-CPWs was also documented.

Acknowledgment

The authors would like to thank H. Braunisch, J. Lee, T. Kamgaing, X. Gu, Y. Kwark, and Z. Zhou for their valuable comments and suggestions.

References

[1] G. Brist, S. Hall, S. Clouser, and T. Liang, "Non classical conductor losses due to copper foil roughness and treatment," in *Proc. Electron. Circuits World Conv.*, Anaheim, CA, USA, Feb. 2005, pp. S19-2-1–S19-2-11.

[2] S. H. Hall, G. W. Hall, and J. A. McCall, *High Speed Digital System Design: A Handbook of Interconnect Theory and Design Practices*. New York, USA: Wiley, 2000.

[3] A. F. Horn, III, J. W. Reynolds, P. A. LaFrance, and J. C. Rautio, "Effect of conductor profile on the insertion loss, phase constant, and dispersion in thin high frequency transmission lines," in *Proc. DesignCon*, Santa Clara, CA, USA, Feb. 2010, no. 5-TA1, pp. 1–22.

[4] S. Hall, S. G. Pytel, P. G. Huray, D. Hua, A. Moonshiram, G. A. Brist, and E. Sijercic, "Multigigahertz causal transmission line modeling methodology using a 3-D hemispherical surface roughness approach," *IEEE Trans. Microw. Theory Tech.*, vol. 55, no. 12, pp. 2614–2624, Dec. 2007.

[5] S. H. Hall and H. L. Heck, *Advanced Signal Integrity for High-Speed Digital Designs*. Hoboken, NJ, USA: Wiley, 2009.

[6] S. G. Pytel, Jr., "Multi-gigabit data signaling rates for PWBs including dielectric losses and effects of surface roughness," Ph.D. dissertation, Dept. Electr. Eng., Univ. South Carolina, Columbia, SC, USA, 2007.

[7] L. Tsang, H. Braunisch, R. Ding, and X. Gu, "Random rough surface effects on wave propagation in interconnects," *IEEE Trans. Adv. Packag.*, vol. 33, no. 4, pp. 839–856, Nov. 2010.

[8] L. Tsang, X. Gu, and H. Braunisch, "Effects of random rough surface on absorption by conductors at microwave frequencies," *IEEE Microw. Wireless Compon. Lett.*, vol. 16, no. 4, pp. 221–223, Apr. 2006.

[9] Q. Chen, H. W. Choi, and N. Wong, "Robust simulation methodology for surface-roughness loss in interconnect and package modelings," *IEEE Trans. Comput. Aided Design Integr. Circuits Syst.*, vol. 28, no. 11, pp. 1654–1665, Nov. 2009.

[10] *HFSS v.12*. (2010) [Online]. Available: http://www.ansys.com/Products/Simulation+Technology/Electromagnetics/High-Performance+Electronic+Design/ANSYS+HFSS

[11] R. N. Simons, *Coplanar Waveguide Circuits, Components, and Systems*. New York, USA: Wiley, 2001.

[12] H. Lawrence, F. Demontoux, J. P. Wigneron, P. Paillou, T. D. Wu, and Y. H. Kerr, "Evaluation of a numerical modeling approach based on the finite element method for calculating the rough surface scattering and emission of a soil layer," *IEEE Geosci. Remote Sens. Lett.*, vol. 8, no. 5, pp. 953–957, Sep. 2011.

[13] J. A. Ogilvy, *Theory of Wave Scattering from Random Rough Surfaces*. Bristol, U.K.: Adam Hilger, 1991.

[14] Q. Li, J. Shi, and K. S. Chen, "A generalized power law spectrum and its applications to the backscattering of soil surfaces based on the integral equation model," *IEEE Trans. Geosci. Remote Sens.*, vol. 40, no. 2, pp. 271–280, Feb. 2002.

[15] S. Hinaga, M. Y. Koledintseva, P. K. R. Anmula, and J. L. Drewniak, "Effect of conductor surface roughness upon measured loss and extracted values of PCB laminate material dissipation factor," in *Proc. Tech. Conf. IPC Expo/APEX*, Las Vegas, NV, USA, Mar.–Apr. 2009, no. S20-2, pp. 1–14.

[16] N. Patir, "A numerical procedure for random generation of rough surfaces," *Wear*, vol. 47, no. 2, pp. 263–277, Apr. 1978.

[17] Y. Z. Hu and K. Tonder, "Simulation of 3-D random rough surface by 2-D digital filter and fourier analysis," *Int. J. Mach. Tools Manufact.*, vol. 32, nos. 1–2, pp. 83–90, 1992.

[18] *MATLAB v.7.12.0.635 (R2011a)*. (2011) [Online]. Available: http://www.mathwork.com/products/matlab/

[19] N. Garcia and E. Stoll, "Monte Carlo calculation for electromagnetic-wave scattering from random rough surfaces," *Phys. Rev. Lett.*, vol. 52, no. 20, pp. 1798–1801, May 1984.

[20] R. F. Harrington, *Time-Harmonic Electromagnetic Fields*. New York, USA: McGraw-Hill, 1961.

Arghya Sain (M'06) received the B.S. degree in electrical engineering from the University of Illinois, Urbana-Champaign, Urbana, USA, in 2010. He is currently pursuing the Ph.D. degree in electrical engineering from the University of Arizona, Tucson, USA.

He joined the High Frequency Packaging and Antenna Design Laboratory, University of Arizona, as a Graduate Research Assistant, in 2011. He is currently investigating techniques to improve bandwidth and signal integrity in interconnects for high-frequency operations. His current research interests include antenna design, microwave circuits (both active and passive), metal surface roughness modeling, semiconductor device physics, and signal integrity.

Kathleen L. Melde (S'84–M'95–SM'97–F'12) received the B.S. degree from California State University, Long Beach, USA, the M.S. degree from California State University, Northridge, USA, and the Ph.D. degree from the University of California, Los Angeles, USA, all in electrical engineering.

She was with the Radar Systems Group, Hughes Electronics, El Segundo, CA, USA, from 1985 to 1996. Her work experience includes diverse projects in the Electromagnetic Systems Laboratory and Solid State Microwave Laboratories, Radar and Communications Sector. She has made contributions to the design and development of antennas and transmit/receive (T/R) modules for airborne phased and active arrays. She has extensive experience in modeling, fabrication and measurement of the performance of antennas, antenna arrays, high-density microwave circuits, and high-speed packaging interconnects. She was a Task Leader for several internal research and development projects. In 1996, she joined the Electrical and Computer Engineering Department, University of Arizona, Tucson, USA, where she is a Professor. Her current projects include tunable RF front ends for cognitive radio, high-speed electronics packaging, on chip antennas, and computational photovoltaics. She has been an Expert Witness and a Consultant in the area of RF circuits and antennas. She has authored over 90 publications and holds five U.S. patents. Her current research interests include applied electromagnetics, antenna theory and design, and microwave circuit design.

Dr. Melde is a member of the Antennas and Propagation (AP-S) and Microwave Theory and Techniques Societies. She is a member of the International Radio Science Union, Eta Kappa Nu, Tau Beta Pi, and Sigma Xi. She was named a University of Arizona College of Engineering Teaching Fellow in 2012. In 2010, she received the Excellence at the Student Interface Award, College of Engineering, University of Arizona. She was a recipient of a 2008 IBM Faculty Award. She has been an invited keynote speaker on several occasions, including at the commencement of the School of Engineering, California State University Northridge, and the conference on the Electrical Performance of Electronic Packages and Systems. From 1999 to 2001, she served on the Administrative Committee for the IEEE AP-S Society. She was an Associate Editor for the IEEE TRANSACTIONS ON ANTENNAS AND PROPAGATION and the IEEE ANTENNAS AND WIRELESS PROPAGATION LETTERS. She is the Co-Chair for the 2012 and 2013 Conference on the Electrical Performance of Electronic Packages and Systems. She is on the Organizing Committee for the 2016 Antennas and Propagation Symposium.